Soft Matter

Soft Matter

COMMUNICATION

Mechanism of anomalously increased oil displacement with aqueous viscoelastic polymer solutions

Andrew Clarke[*a], Andrew M Howe[a], Jonathan Mitchell[a], John Staniland[a], Laurence Hawkes[a], Katherine Leeper[a]

Single-phase flow of viscoelastic polymer solutions in both microfluidic devices and rock cores exhibit apparent flow thickening. We demonstrate that this thickening occurs above a critical Deborah number corresponding to the onset of spatio-temporal fluctuations. These fluctuations are observed to occur over a broad range of spatial and temporal scales consistent with elastic turbulence. The fluctuations provide a previously unreported mechanism for enhancing the displacement of a second, capillary trapped, immiscible phase.

Fluid flows in porous media display a variety of physical phenomena and are key to many natural and commercial processes spanning multiple fields from geophysics through chemical engineering to medicine. In most important situations, the pore length scale is small and the viscosity of the liquid high such that the Reynolds number is very small, typically $Re < 10^{-2}$. Hence there is a general expectation resulting from Stokes' analysis that single-phase flows will be dominated by viscous forces [1] and, whilst spatially non-uniform from pore-to-pore [2], will be time-invariant [1]. For single-phase flow this limit corresponds to Darcy's law [3]. However, many pore-scale transport problems involve multiple fluid phases where one of the phases is immobile and the mechanism of mobilisation is of primary interest. When a second immiscible phase becomes trapped by capillary forces, and after transients and shocks have propagated through the system, the only forces generally available to induce displacement of the trapped phase are gravity and a pressure gradient induced by an imposed flow of the mobile phase [4] [5]. Importantly, there are literature examples of displacement in porous structures that are not explained by these concepts which involve a trapped (oleic) phase displaced by a mobile (aqueous) polymeric solution [6]. Here we demonstrate the existence of additional flow processes, induced by elasticity due to the presence of flexible polymers, which cause mobilisation of a trapped immiscible phase. Such mechanisms have significant ramifications for groundwater remediation, CO_2 storage and lab-on-a-chip devices. In addition, they have an obvious application for enhanced oil recovery: the context a topic of considerable industrial importance [4,5,6,7,8] that provides the background to our work.

Aqueous polymer solutions are used in a variety of applications to modify flow. Here we focus on their use to enhance oil recovery from reservoirs already depleted using water injection. Introducing an aqueous polymer solution increases the displacing phase viscosity such that previously bypassed oil phase (due to rock heterogeneity or to fingering instability) is displaced, i.e. creating a change in the macroscopic flow distribution. Nevertheless, microscopically, where the aqueous phase has flowed, remaining trapped oil phase exists as disconnected regions over a range of length scales [9]; such regions are termed "ganglia". To remove an additional proportion of the trapped phase from the medium using an aqueous phase, the pressure gradient generated by the viscous flow must exceed the capillary trapping force [4,9]. When ganglia start to move, in addition to translating they can break into smaller ganglia which in turn can re-trap. The smaller ganglia, for given capillary trapping force, require a higher pressure gradient to move. This balance of forces is characterised by the capillary number, Ca, (using Darcy's law, $Ca = k\nabla P/\gamma$ with k the permeability, ∇P the pressure gradient and γ, the interfacial tension). Accordingly, if the capillary number remains below a threshold, no further displacement of the immiscible phase is expected once the ganglia have become disconnected and trapped, [4,9] . The capillary number for displacement of ganglia, in a statistical sense, depends on the droplet size distribution which, for a general rock, is unknown. The details have been discussed by Armstrong et al [10], where an appropriate statistical definition (only accessible by computed micro-tomography) gives Ca~1 for the threshold as expected. The simplistic definition that is generally used, and that we also use, ignores a length scale ratio (which in general is experimentally inaccessible) and thus displacement occurs between Ca~10^{-5} and Ca~10^{-3} depending on wettability state of the system [4].

Traditionally, polymer solutions were thought only to improve flow homogeneity and thereby recovery of bypassed oil, whilst leaving the residual "saturation" (the averaged volume fraction of trapped phase, i.e. ganglia within the porous structure) unaltered [5, 8]. Recently the idea that viscoelastic solutions of flexible polymers cause movement of the trapped phase at capillary numbers lower than the expected critical value has been proposed [11]. However, until now, no coherent mechanism has been put forward to explain the latter claim, which remains a subject of intense debate.

In this communication we use microfluidic networks (micromodels) to show that as a function of flow rate, for polymer solutions with sufficient elasticity, there is a transition from steady laminar flow to a strongly fluctuating flow, consistent with previous observations of elastic turbulence [12,13,14]. Elastic turbulence is a low Reynolds number phenomenon (here $Re<10^{-2}$) arising in this case through a long characteristic relaxation time of the polymer molecules in solution. We find in addition that these flow fluctuations cause menisci of a trapped immiscible phase to fluctuate. We show that the menisci, in an equivalent non-elastic flow, are stationary. Furthermore the fluctuating menisci are seen to induce mobilisation of trapped ganglia, otherwise described as capillary desaturation. Thus the onset of elastic fluctuations, causing destabilisation of trapped ganglia, is the mechanism underpinning the observed additional immiscible phase mobilisation driven by viscoelastic polymer solutions.
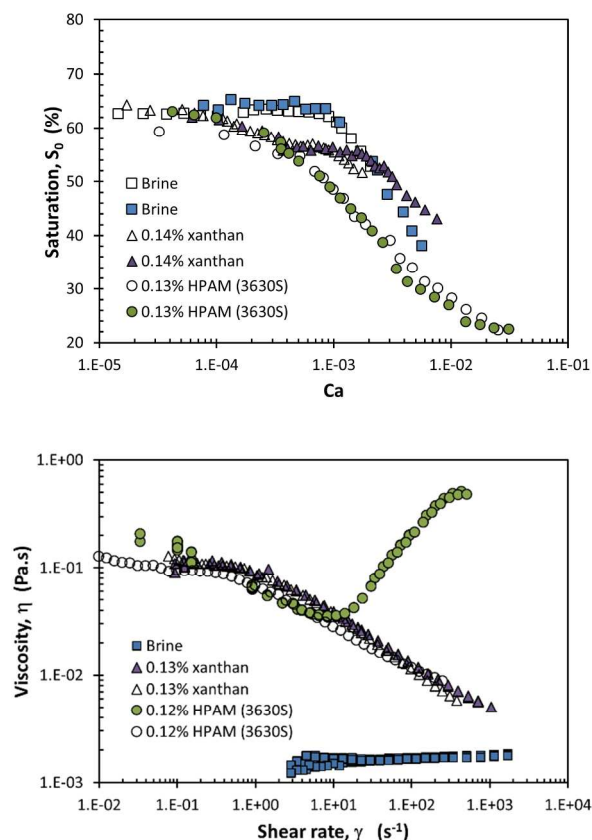

Fig. 1 (a) Saturation of oil as a function of capillary number using three fluids, each displacing oil from Bentheimer sandstone. Open symbols denote repeat experiments to illustrate the material repeatability. HPAM is seen to unexpectedly reduce saturation of oil at a significantly lower capillary number ($Ca\sim3x10^{-4}$) than brine or xanthan ($Ca\sim1x10^{3}$). (see text for detailed description) (b) Viscosity at 20°C measured using a rheometer (open symbols) and derived from pressure gradient measurement in flow through a Bentheimer sandstone sample (solid symbols). The xanthan and HPAM

rheometer data (open symbols) overlay, whereas the derived apparent viscosities (filled symbols) do not.

The macroscopic effect is illustrated in Fig. 1. A sequence of liquids was flowed into a cylindrical rock sample (Bentheimer, a relatively uniform sandstone with mean pore throat, i.e. pore-to-pore channel, size 39μm) to mimic the industrially employed oil-recovery procedure. The sample is first saturated with brine, then oil (34mPas, PSL Rheotek, S20) is injected to fill the pore space. This procedure ensures the mineral surfaces are predominantly wetted by the aqueous phase, which was verified by NMR relaxation time analysis. A brine (78 mM ionic strength, pH ≈ 8, which provides the medium for all the aqueous solutions described here) was then flowed until no further change in the remaining oil saturation was observed. This was the initial state from which we compared subsequent removal of oil using a selection of aqueous solutions injected over a range of *Ca* (interfacial tension is not varied across any of the experiments and was not affected by the chosen polymers [15]).

At each stage of the procedure the oil and brine saturations (volume fractions) were measured in situ using a low-field NMR spectrometer [16]. In Fig. 1(a) we compare resulting saturation as a function of *Ca* for brine, xanthan, and partially hydrolysed polyacrylamide (HPAM; SNF-Floerger, Flopaam 3630S, molecular mass Mw ~ 18 MDa). We have also used HPAM 3130S, Mw ~3.5MDa and 6040S, Mw ~ 30MDa. In Fig. 1(b) we compare the measured shear viscosity of 3630S and xanthan obtained in a rheometer (Malvern Gemini NanoHR using a C2.3/26 bob-and-cup measuring geometry) with the apparent viscosity deduced from measurements of the differential pressure across the rock sample during single-phase flow using Darcy's law (apparent viscosity $\eta = kA\nabla p / q$, and apparent shear-rate $\dot{\gamma} = q / A\sqrt{k\phi}$, with *A* the sample cross sectional area, *q* the volumetric flow rate and ϕ the porosity). All solutions were prepared to give a low-shear viscosity, $\eta(0)$, of approximately 100mPas unless specified. The polymer concentrations were chosen to give similar low-shear viscosity, which for HPAM 3630S is a factor of is 15× more concentrated than the overlap concentration, c* (c*=0.008wt% for HPAM (3630S)). The value of c* is based on an experimental definition [17].

The data in Fig. 1 demonstrate that, contrary to expectation [4,9], HPAM (3630S) causes rapid desaturation from a lower critical capillary number than brine or xanthan. We see the onset of rapid desaturation with HPAM at $Ca\sim3x10^{-4}$, whereas for brine rapid desaturation begins at $Ca\sim1x10^{-3}$. For xanthan, rapid desaturation begins for *Ca* between $1x10^{-3}$ and $1.5x10^{-3}$. Both the xanthan and HPAM data deviate from the brine data initially. We believe this is due to the very much higher ratio of the injected polymer solution viscosity to oil viscosity (3:1) compared to that for brine injection (1:34). Lenormand [18] has demonstrated the change in microscopic configuration of trapped phase as a function of the viscosity ratio. Note that the point at which the xanthan data depart from the HPAM data, corresponds to the apparent shear rate at which the HPAM begins to show apparent flow thickening, already suggesting a linkage between the two phenomena.

For single phase flow within the core, above a particular flow rate, an enhanced pressure drop is observed for HPAM (3630S) which appears as an enhanced apparent viscosity in Fig. 1b. This excess pressure has previously been associated with increased extensional viscosity due to complex, but steady, flows generated by expansions and contractions within the porous structure [19]. However, such an

increase in extensional viscosity will simply add to the pressure gradient for flow in a porous medium and hence be captured in the capillary number defined for Fig. 1a. Thus an enhancement in extensional viscosity cannot explain the additional oil displacement, i.e. from a lower critical capillary number as seen in Fig. 1a.
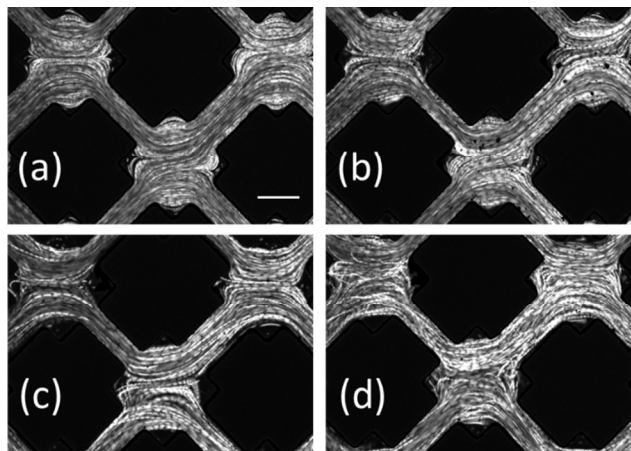

Fig. 2 Streak photographs of flow, $q = 12$ min-1 ($=22.2s^{-1}$). (a) 84 wt% glycerol, (b) 0.24 wt% xanthan. (c) 0.24 wt% HPAM 3630S, (d) 0.12 wt% HPAM 6040S. Flow is left to right. The scale bar in (a) represents 100µm. (a) and (b) exhibit laminar flow whilst (c) and (d) exhibit crossing streaklines and fluctuating flow. Solutions (b), (c) and (d) have nominally the same low-shear viscosity (1Pas), while the Newtonian glycerol solution has a viscosity of ~75mPas).

We probe the details and origin of the flow features illustrated in Fig. 1 using a 2D analogue microfluidic network. The pores are 200 µm square and the connecting channels are normally distributed around 75 µm width with a lower cut-off at 50 µm and an upper cut-off at 150 µm. The channels are 100 µm deep. The pore structure as supplied (Epigem Ltd) has an internal surface of SU8 photopolymer and is oleophilic. For the two-phase experiments (Fig 4. below) we chemically modified the internal surface to be hydrophilic and hence comparable to Bentheimer. Note that whereas the wettability affects the detailed configuration of the trapped phase, it does not change the onset of fluctuations in the aqueous phase, nor the ability of those fluctuations to mobilise trapped phase. We observe streaklines using 1 µm polystyrene particles (Sigma-Aldrich) seeded in the flow of four solutions ((a) 84 wt% glycerol – Newtonian, 100mPas; (b) 1Pas xanthan - pseudoplastic; (c) 1Pas HPAM 3630S - viscoelastic; (d) 1Pas HPAM 6040S - viscoelastic), see Fig. 2. These four liquids have significantly different relaxation times in flow. Here we choose to take the relaxation time, λ, from the convected Maxwell model as

$$\lambda = \frac{1}{2} \frac{N_1}{\dot{\gamma}\sigma} \qquad (1)$$

where N_1 is the first normal stress difference, $\dot{\gamma}$ the shear rate and σ the shear stress; all directly measured in the rheometer. The Deborah number, De, characterises the extent to which the response of a liquid to a deformation is viscoelastic ($De>1$) rather than purely viscous ($De<1$). Thus, for the flow rate in Fig. 2, the Deborah numbers $De=\lambda u/l$ based on the average flow velocity u, the relaxation time, λ and the pore-to-pore length-scale l, are $De = 0$ for glycerol, $De \approx 0.06$ for xanthan, $De \approx 2.5$ for HPAM 3630S and $De \approx 8.3$ for HPAM 6040S, whilst Re remains fixed at Re ~ 10^{-4}. Hence we expect the flows of HPAM to behave visco-elastically whereas the flows of glycerol and xanthan should be viscous only.

Whereas the above definition of relaxation time is strictly valid only for dilute systems, we use it here since we observe that the fluctuation onset is related to a concentration independent (but strongly molecular weight dependent) characteristic time (i.e. molecular time) and not the linear viscoelastic relaxation time as assumed by other workers. This can also be seen in the data of Fig. 5. However, the full details of these observations are beyond the scope of the present communication, and will be published separately [15].

Previous studies of entry flow for similar materials [20] have defined an elasticity number $EI=Wi/Re$, with Wi the Weissenberg number, as characterising the observed instabilities. EI characterises the ratio of elastic and inertial forces. Here we have a Reynolds number Re=10^{-4} (see fig 4. below), i.e. negligible inertia and thus the Deborah and Weissenberg numbers are expected to characterise the flow. Moreover, Pakdel and McKinley [21] define $M=\sqrt{(De.Wi)}$ as characterising the onset of elastic turbulence. We examine the implications of this for the present porous flow system in detail in [15].

In Fig. 2 it is very clear that, for both the 3630S and the 6040S solutions, crossing streaklines are observed consistent with the onset of elastically induced flow fluctuations [13]. In contrast, the Newtonian glycerol and shear-thinning xanthan solutions exhibit no such streakline crossings. Exploring this behaviour further with 3630S solution, we observe temporal and spatial flow fluctuations starting from flow rates above $q \approx 9$ µl.min^{-1} ($De = 2.6$). Qualitatively, crossing streaklines are seen above a threshold flow rate commensurate with a significant increase in the measured pressure gradient.
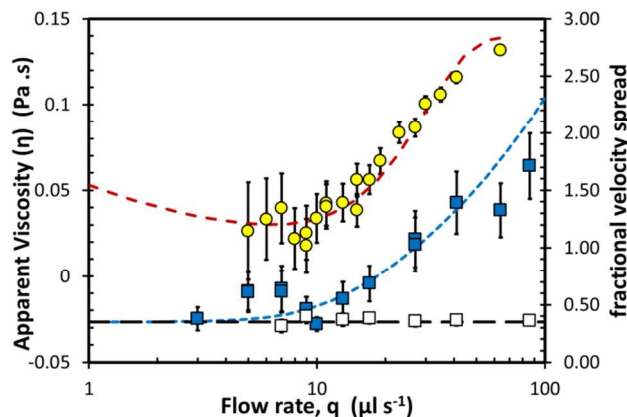

Fig. 3 Circles: apparent viscosity derived from pressure gradient during flow in the microfluidic network. Squares: range of velocities observed in the sampled region (approx. 100 µm square in centre of pore) for 84 wt% glycerol (open squares) and HPAM 3630S (filled squares). Example particle tracking images and time traces can be found in supplementary material. It is observed that the onset of apparent flow thickening on increasing flow rate coincides with the onset of increasing flow fluctuations.

We study the instability onset in greater detail by tracking the polystyrene particles seeded in the flow and extracting the scale of velocity fluctuation at a position in the middle of a pore for both a Newtonian liquid (84 wt% glycerol) and the polymer solution (HPAM 3630S). The results are shown in Fig. 3. The observed fractional velocity spread (the range of measured velocities observed during a time interval divided by the average velocity) for the glycerol solution is finite because of the steady state range of

velocities in the sampled region. For the Newtonian liquid the value does not vary with flow rate. For the viscoelastic liquid (HPAM 3630S) there is observed a strong increase in temporal velocity fluctuation at a flow rate commensurate with a strong increase in the pressure gradient in the microfluidic network. We have not yet investigated in detail the spatial correlation of the observed fluctuations, here we merely note that menisci fluctuating in adjacent pores (see below) are uncorrelated. These observations are consistent with recent work by Burghelea et al. [22] in which both a transition to strong fluctuations and a concomitant sudden increase in the pressure gradient was seen for sinuous-pipe flow. Comparing with Fig. 1(b), we see the same onset of apparent flow thickening in the Bentheimer rock sample. However, the apparent shear rate at which thickening occurs is at lower values in the rock ($\approx 9s^{-1}$) than in the microfluidic network ($\approx 16s^{-1}$). In addition to flow and material properties, we expect the onset of fluctuations to be dependent on a ratio of length scales in the geometry [21]. We therefore attribute this difference to the differing ratio of length scales (shear, curvature) between the microfluidic network and the core.
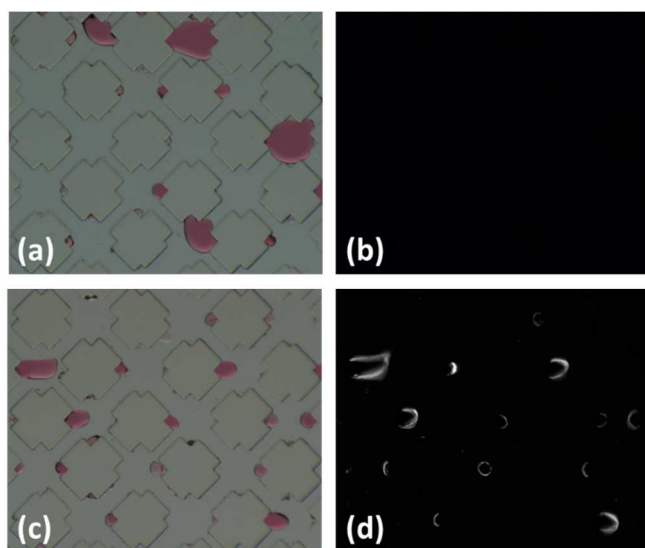

Fig. 4 Images of oil ganglia remaining after polymer flow at q = 60 µl min^{-1} (=111s^{-1}). (a) and (b) 0.24 wt% xanthan ($De\approx0.3$), (c) and (d) 0.24 wt% HPAM 3630S ($De\approx12$). (a) and (c) are still images with oil dyed red; (b) and (d) are integrated difference images of respective video sequences (see supplementary material). Flow is left to right. We see that for the HPAM flow (c) and (d) there are significant fluctuations of the menisci which are absent in the xanthan case (a) and (b).

Capillary desaturation of porous structures where the aqueous phase exhibits elastic turbulence has not been previously reported. To compare with the rock data above (Fig. 1), we first fill the microfluidic network with the same oil (dyed red with oil-red EGN) and then flow brine at a low rate until there is no further movement of the trapped oil. We subsequently inject our test solution at a sequence of increasing flow rates, at each step flowing until no further displacement of the remaining oil is seen. In Fig. 4 we compare images of saturation for xanthan solutions and HPAM (3630S) at similar capillary number (Ca = 4 × 10^{-2}) and Reynolds number (Re = 1.3 × 10^{-4}). We also show constructions where differences of successive captured images are summed to highlight the temporal displacement of menisci. For the xanthan solution, the menisci are stationary, whereas for HPAMs they fluctuate strongly. We interpret the meniscus fluctuations as being driven by fluctuations in stress caused by aqueous-phase flow fluctuations as in single-phase flow (Figs 2 and 3).

In Fig. 5 we compare the observed onset of desaturation with the observed onset of fluctuations for two microfluidic network geometries (described in SI) and for Bentheimer rock. Here we have chosen to plot the average local aqueous-phase velocity. The fluctuation onset velocity is then simply calculated from the flow rate. To estimate the average local velocity in the two-phase situation we again use the aqueous-phase flow rate, but scaled to account for the oil saturation. In the plot we see that the aqueous-phase velocity for onset of desaturation is the same as that for the onset of fluctuations, except for the case of microfluidic network MM1. In MM1, fluctuations do not start until *after* the point at which desaturation due to the static pressure gradient commences. Hence, provided the fluctuations occur before the corresponding static pressure gradient desaturation, the onset of desaturation coincides with the onset of fluctuations.

We now consider how the fluctuations might interact with trapped oil ganglia. Oil-bearing rocks with a wide range of wettabilities exist. If water wet (the case illustrated by Bentheimer and treated microfluidic networks), then the surfaces have a complete covering of a water film and no three-phase contact line exists. Ganglia-trapping is then solely due to the excess capillary pressure required to move menisci through pore-to-pore constrictions (i.e. pore-throats).
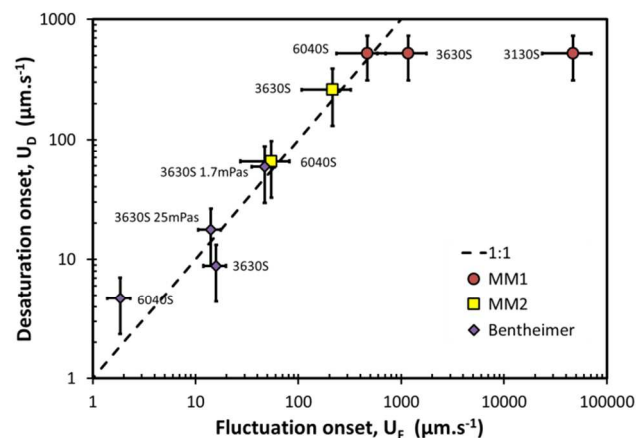

Fig. 5 Comparison of average local velocity for onset of desaturation and for onset of fluctuations. Circles are data for a microfluidic network (MM1) structure where channels were aligned with the average flow direction, squares are for the microfluidic network shown in Fig. 4 (MM2), and diamonds are data from Bentheimer sandstone. Fluctuation onset in the sandstone is identified at the point of upturn in the apparent viscosity. For both 2D and 3D systems there is a striking correspondence between fluctuation onset and desaturation onset.

If the pore system is mixed wet, then three-phase contact lines exist. A sessile drop on a surface in thermodynamic equilibrium with that surface and the surrounding liquid will be displaced by any force acting on the drop tangential to the surface. However, drops on surfaces are not in general in thermodynamic equilibrium. Practically, this latter manifests as a difference between the "advancing" and "receding" values of contact angle. This difference - the hysteresis - requires a net force to be exceeded before the drop will move. Thus wetting-line hysteresis also provides a capillary force that needs to be overcome for ganglion displacement. Wetting hysteresis will, in general, arise from both surface roughness and chemical heterogeneity.

In either trapping scenario, it should be expected that fluctuations in the aqueous flow field will give rise to additional stress fluctuations which, if large enough, will initiate either displacement of menisci

Soft Matter

though constrictions or movement of contact lines [23]. Those displacements or movements cause trapped phase mobilisation, and hence oil desaturation, at lower capillary numbers than expected through consideration of the steady state pressure gradient generated by steady viscoelastic flow alone. Note that the measured size of fluctuations with respect to mean velocity (Fig. 3) scales with flow rate above onset and are O(1) in velocity ratio at 3× the onset flow rate. For a viscous system this observation implies pressure gradient fluctuations are also of O(1). In our systems elastic forces are expected to increase the stress fluctuations still further.

In addition to trapped-phase mobilisation, strong aqueous-phase fluctuations can also lead to emulsification [24]. If the generated droplets are smaller than pore throats then transport through the porous medium as part of the aqueous phase is expected. Droplet formation within channels has been the subject of extensive study over the last decade, since control of this process leads to a manufacturing route for monodisperse droplets. In general, drop formation is a capillary driven process which, depending on flows and material properties, is either absolutely or convectively unstable. In both cases, flow fluctuations have the potential to enhance emulsification processes and thereby provide an additional desaturation mechanism. Drop formation has been observed in our microfluidic network experiments.

Conclusions

We have shown that viscoelastic polymer solutions can anomalously desaturate a porous medium, i.e. displacement of the trapped phase can occur at lower than expected capillary number. Furthermore, our experiments show that the onset of this anomalous desaturation coincides with the onset of temporal flow fluctuations. These flow fluctuations have the same behaviour as elastic turbulence. As the Deborah number of the injected flow increases, a critical value is reached at which temporal flow fluctuations start, in turn generating a bath of pressure fluctuations capable of providing sufficient additional force to release or disrupt ganglia of a trapped immiscible phase. The additional work required to drive the fluctuations appears as an anomalous increase in pressure gradient which is conventionally described as flow thickening within a Darcy framework. Whereas flow thickening is, in a Darcy framework, advantageous for trapped phase displacement, such an interpretation does not describe in full the additional mobilisation seen when expressed in terms of capillary number. Thus flooding with high Mw viscoelastic polymer solutions can generate flow fluctuations which enhance oil recovery beyond that describable with conventional, i.e. Darcy based, considerations.

Notes and references

a Schlumberger Gould Research, Madingley Road, Cambridge, UK, CB3 0EL. email: andrew.clarke@slb.com

1 J. S. Andrade Jr., U. M. S. Costa, M. P. Almeida, H. A. Makse and H. E. Stanley, *PRL*, 1999, **82**(26), pp. 5249

2 S. S. Datta, H. Chiang, T. S. Ramakrishnan and D. A. Weitz, *PRL*, 2013, **111**, 064501

3 J. Bear, Dynamics of Fluids in Porous Media, New York: Dover, 1988.

4 L. W. Lake, Enhanced Oil Recovery, Prentice-Hall, 1989.

5 J. Beaumont, H. Bodiguel and A. Colin, *Soft Matter*, 2013, **9**, 10174-10185

6 Z. Zhang, J. Li and J. Zhou, *Transp Porous Media*, 2011, **86**, 199; E. C. Vermolen, M. J. T. Haasterecht and S. K. Masalmeh, *SPE Journal*, 2014, SPE-169681.

7 R. S. Seright, T. Fan, K. Wavrik and R. d. C. Balaban, *SPE Journal*, 2011, SPE-129200; D. H. Kim, S. Lee, C. H. Ahn, C. Huh and G. A. Pope, *SPE Journal*, 2010, SPE-129971.

8 C. Huh and G. A. Pope, *SPE Journal*, 2008, SPE-113417.

9 S. S. Datta, T. S. Ramakrishnan and D. A. Weitz, *Physics of Fluids*, 2014, **26**, 022002.

10 R.T.Armstrong, A.Georgiadis, H.Ott, D.Klemin, S.Berg, *Geophysical research letters*, 2014, 41, 55–60

11 D.Wang, G.Wang, H.Xia, *SPE Journal*, 2011, SPE-144294; D. Wang, H. Xia, S. Yang and G. Wang, *SPE Journal*, 2010, SPE-127453

12 A. Groisman and V. Steinberg, *Nature*, 2000, **405**, 53; A. N. Morozov and W. van Saarloos, *Physics Reports*, 2007, **447**, 112; Marc-Antoine Fardin and Sandra Lerouge, *Soft Matter*, 2014, **10**, 8789

13 J. Zilz, R. J. Poole, M. A. Alves, D. Bartolo, B. Levache and A. Linder, *Journal of Fluid Mechanics*, 2012, **712**, 203.

14 A. Groisman, S.R.Quake, *PRL*,2004, **92**(9), 094501

15 *Soft Matter*, in preparation.

16 J. Mitchell, T. C. Chandrasekera, D. J. Holland, L. F. Gladden and E. J. Fordham, *Physics Reports*, 2013, **526**(3), 165

17 M.Rubenstein, R.H.Colby, Polymer Physics, OUP Oxford, 2003

18 R.Lenormand, E.Touboul, C.Zarcone, *J. Fluid Mech*. 1988, **189**, 165-187

19 D. Delshad, D. H. Kim, O. A. Magbagbeola, C. Huh, G. A. Pope and F. Tarahhom, *SPE journal*, 2008, SPE-113620

20 L.E. Rodd, J.J. Cooper-White, D.V. Boger, G.H. McKinley, *J. Non-Newtonian Fluid Mech*. 2007, **143,** 170–191

21 P. Pakdel and G. H. McKinley, *PRL*, 1996, **77**(12), 2459

22 T. Burghelea, E. Segre, I. Bar-Joseph, A. Groisman and V. Steinberg, *Phys. Rev. E*, 2004, **69**, 066305

23 Y. D. Shikhmurzaev and J. E. Sprittles*, J. Fluid Mech*., 2012, **694**, 39

24 R. J. Poole, B. Budhiraja, A. R. Cain and P. A. Scott, *Journal of Non-Newtonian Fluid Mechanics*, 2012, (**177-178**), 15

Soft Matter Accepted Manuscript

Graphical abstract

Trapped oil (red)   Meniscus fluctuations

254x190mm (96 x 96 DPI)